Victor V. Kotlyar
Alexey A. Kovalev
Anton G. Nalimov

Optical Hall Effect in the Sharp Focus of Laser Light

Springer

Optical Hall Effect in the Sharp Focus of Laser Light

Victor V. Kotlyar · Alexey A. Kovalev ·
Anton G. Nalimov

Optical Hall Effect in the Sharp Focus of Laser Light

Springer

Victor V. Kotlyar
Image Processing Systems Institute
National Research Center
Kurchatov Institute
Samara, Russia

Alexey A. Kovalev
Department of Technical Cybernetics
Samara National Research University
Samara, Russia

Anton G. Nalimov
Image Processing Systems Institute
National Research Center
Kurchatov Institute
Samara, Russia

ISBN 978-3-031-64682-9 ISBN 978-3-031-64683-6 (eBook)
https://doi.org/10.1007/978-3-031-64683-6

This Springer imprint is published by the registered company Springer Nature Switzerland AG
The registered company address is: Gewerbestrasse 11, 6330 Cham, Switzerland

Preface

Since ancient times, mankind has been able to focus light with the help of lenses and mirrors. At the focus, not only is the energy of light concentrated, but all six projections of the electromagnetic field vectors are added at the focus, forming complex three-dimensional distributions of amplitude, phase, and polarization states. Recently, many interesting optical effects have been discovered in a sharp focus of coherent laser radiation: rotation of polarization vectors only in the longitudinal plane—photon wheels; the presence of points and lines of polarization singularity, in which the direction of the linear polarization vector is not determined; the reverse flow of light energy, when the longitudinal projection of the Poynting vector is directed in the opposite direction with respect to the direction of propagation of the focused light; spin-orbit conversion, when a transverse energy flux is formed at the focus of a Gaussian beam with circular polarization, which can rotate a microparticle along a circular trajectory. Another interesting effect that has recently been discovered in the focus of laser light is the optical Hall effect. The usual Hall effect consists in a transverse displacement, in different directions, in a magnetic field of charges of different signs or different spins, which carry an electric current. In optics, particles with different spins correspond to light beams with left and right circular polarizations. Therefore, the optical spin Hall effect in focus consists in the formation of regions separated in space, in which light has a different direction of elliptical or circular polarization.

The book will be of interest to a wide range of scientists, engineers working in the field of optics, photonics, laser physics, optoinformation technologies, and optical instrumentation. It can also be useful for bachelors and masters in the specialties applied mathematics and physics, applied mathematics and informatics, optics and graduate students specializing in these areas.

Samara, Russia

Victor V. Kotlyar
Alexey A. Kovalev
Anton G. Nalimov

Introduction

The Hall effect consists in the occurrence of a transverse voltage (Hall voltage) in a metal conductor at the edges of a sample placed in a transverse magnetic field when a current flows perpendicular to the field. Hall voltage was discovered by Edwin Hall in 1879, and the effect is named after him. Due to the many types of Hall effects, for clarity, the original effect is sometimes referred to as the ordinary Hall effect to distinguish it from other types that may have additional physical mechanisms. In semiconductors, the Hall effect leads to separation of electrons and holes in space. Note that electrons and holes have different spins. In the absence of a magnetic field in non-magnetic conductors, current carriers with opposite directions of spins can be deflected in different directions perpendicular to the electric field. This phenomenon, called the spin Hall effect, was theoretically predicted by Dyakonov and Perel in 1971. There are external and internal spin effects. The first of them is associated with spin-dependent scattering, and the second, with spin-orbit interaction. The spin Hall effect is closely related to another interesting effect, the Magnus effect. The Magnus effect was discovered by Heinrich Magnus in 1853 and occurs when a liquid or gas flows around a rotating body. In this case, a force acting perpendicular to the flow acts on the body. This phenomenon is often used in sports, for example, a dry leaf football kick, as well as in a twisted serve in table tennis (a spinning tennis ball deviates from a straight line). In optics, an effect similar to the Magnus effect was discovered in multimode fibers in 1990 by Zel'dovich B. Ya. It was shown that the vortex modes of a fiber with left and right circular polarization propagate at different angles to the optical axis of the fiber. In 1992, A. V. Volyar discovered a similar Magnus effect in uniaxial crystals. The spin Hall effect in optics was discovered later. In 2004, Onoda M. et al. theoretically showed that when reflected from the interface between two media, linearly polarized light is divided into two beams with left and right circular polarization, propagating at different angles to the surface. In 2005, Kavokin A. experimentally observed the optical spin Hall effect during the passage of light with linear polarization through a multilayer structure. In the transmitted light, the regions with left and right circular polarizations were separated in space. The theory of optical effects of Magnus and Hall based on the geometric phase of Berry and spin-orbit interaction was developed in 2004 by Bliokh K. Y. The geometric phase of Berry

(1984) as applied to light with circular polarization consists in the fact that light with circular polarization, passing the same distance in a gradient medium with light with linear polarization, acquires an additional phase incursion. Also, between the light with left circular and right circular polarizations, an additional phase delay can occur. This leads to the fact that in a gradient (or other inhomogeneous) medium, light with left and right circular polarizations can propagate along different paths and be separated in space. The question arises: Can the optical Hall effect manifest itself not due to the interaction of light with the medium, but when propagating in free space, for example, in a sharp focus? In 1992, Allen L. et al showed that an individual photon has an orbital angular momentum. And in 2011, Bliokh K. et al. showed that spin-orbit conversion takes place in a sharp focus of light. That is, even at the focus, one can find the conditions under which the Hall effect occurs.

This book is devoted to the optical Hall effect in the sharp focus of laser radiation. On the basis of the theory of Richards-Wolf (1959), which adequately describes the behavior of light at the focus, many specific examples of light fields show that both spin and orbital Hall effects take place near the focus. In this case, there can be many regions with left and right circular polarization at the focus. Their number depends on some parameter of the focused beam. The spin Hall effect is when local regions are formed in the plane of focus (or near it), in some of which the light has a right elliptical polarization, and in others it has a left one. In this case, in the initial plane, the light had linear polarization at each point. The orbital Hall effect appears when there are local areas in the plane of focus, in some of which the transverse energy flow rotates clockwise, and in others—counterclockwise. In the simplest case, the spin Hall effect occurs when a linearly polarized Gaussian beam is focused. In this case, four local regions are formed near the focus (before and after, but not in the focus itself), in which the light has a left-hand elliptical polarization along one diagonal, and a right-hand polarization along the other diagonal. The spin and orbital Hall effects also arise at the focus of light fields with non-uniform linear polarization, when at each point in the beam cross section the polarization is linear, but changes its direction from point to point. For such cylindrical vector fields, under certain conditions, the Hall effect occurs at the focus itself, and for other beam parameters, near the focus. For such beams, the presence or absence of the Hall effect at the focus is associated with the absence or presence of polarization singularity points in the initial light field.

The authors are grateful for the numerical simulation by Ph.D. Stafeev S. S. and Ph.D. Kozlova E. S.

The results included in the monograph were supported by the Russian Science Foundation grant 23-12-00236.

Contents

About the Authors

Victor V. Kotlyar is a head of Laboratory at the Image Processing Systems Institute of National Research Center, Kurchatov Institute, Samara, Russia and professor of Computer Science department at Samara National Research University. He received his MS, Ph.D., and Dr.Sc. degrees in Physics and Mathematics from Samara State University (1979), Saratov State University (1988) and Moscow Central Design Institute of Unique Instrumentation, the Russian Academy of Sciences (1992). He is co-author of 400 scientific papers, five books and seven inventions. e-mail: kotlyar@ipsiras.ru

Alexey A. Kovalev (b. 1979) graduated (2002) from Samara National Research University, majoring in Applied Mathematics. He received his Doctor in Physics and Maths degree in 2012. He is a senior researcher of Laser Measurements laboratory at Image Processing Systems Institute National Research Center, Kurchatov Institute, Samara, Russia and professor of Computer Science department at Samara National Research University. He is a co-author of more than 200 scientific papers. e-mail: alanko@ipsiras.ru

Anton G. Nalimov (b. 1980) graduated from Samara State Aerospace University in February, 2003. Entered in postgraduate study in 2003, finished it in 2006 with speciality 01.04.05 "Optics". A. G. Nalimov works on Technical Cybernetics department in Samara National Research University as an associate professor, works as a scientist in the Image Processing Systems Institute of National Research Center, Kurchatov Institute, Samara, Russia. Candidate in Physics and Mathematics, co-author of 100 papers and three inventions. e-mail: anton@ipsiras.ru

Chapter 1
Spin Hall Effect at the Focus for Light with Linear Polarization

1.1 Circular Polarization Near the Tight Focus of Linearly Polarized Light

Sharp focusing of laser radiation is understood as the focusing of light by lenses with a high numerical aperture, and it is no longer possible to neglect the vector nature of the light wave. In this case, to calculate the light field at the focus, it is necessary to take into account all the components of the strength of the electric and magnetic field of the light wave. The classical formulas for calculating the light field in a sharp focus were obtained by Richards and Wolf in [1].

At present, a large number of works are devoted to the sharp focusing of light. However, most of the works are devoted to studying the behavior of the intensity at the focus, for example, obtaining focal spots of various shapes [2–7]. Much less work is presented on the study of other characteristics of the light field, such as the energy flux (Poynting vector) [8–10], spin or orbital angular momentum [11–14]. We also note that the main attention of researchers is focused on the study of the behavior of light directly in focus; less attention is paid to the behavior of light at some distance from the plane of sharp focus.

In this section, the sharp focusing of linearly polarized light is considered. It was shown that, with distance from the focal plane, regions arise in which the polarization ceases to be linear. In this case, when passing through the plane of focus, the direction of polarization in these regions changes to the opposite—in regions with right circular polarization, the direction changes to left circular and vice versa.

1.1.1 Theoretical Background

In [1], expressions were obtained for the projections of the electric field strength vector at the focus of the aplanatic system. The Jones vector for an initial field with

V. V. Kotlyar et al., *Optical Hall Effect in the Sharp Focus of Laser Light*,
https://doi.org/10.1007/978-3-031-64683-6_1

linear polarization directed along the y-axis has the form:

$$\boldsymbol{E}_{\text{lin}} = A(\theta)\begin{pmatrix}0\\1\end{pmatrix} \tag{1.1}$$

and the projections of the vector of the electric field strength and magnetic field strength near the focus for the initial field (1.1) have the form:

$$\begin{aligned}
E_x &= -iI_{2,2}\sin 2\varphi,\\
E_y &= -i\big(I_{0,0} - I_{2,2}\cos 2\varphi\big),\\
E_z &= -2I_{1,1}\sin\varphi,\\
H_x &= i\big(I_{0,0} + I_{2,2}\cos 2\varphi\big),\\
H_y &= iI_{2,2}\sin 2\varphi,\\
H_z &= 2I_{1,1}\cos\varphi,
\end{aligned} \tag{1.2}$$

where

$$I_{\nu,\mu} = \left(\frac{4\pi f}{\lambda}\right)\int_0^{\theta_0}\sin^{\nu+1}\left(\frac{\theta}{2}\right)\cos^{3-\nu}\left(\frac{\theta}{2}\right)\cos^{1/2}(\theta)A(\theta)\mathrm{e}^{ikz\cos\theta}J_\mu(x)\mathrm{d}\theta \tag{1.3}$$

where λ is the wavelength of light, f is the focal length of the aplanatic system, $x = kr\sin\theta$, $J\mu(x)$ is the Bessel function of the first kind, and $\mathrm{NA} = \sin\theta_0$ is the numerical aperture. The angle φ in Eq. (1.2) is the conventional polar (or azimuthal) angle in the transverse planes, including the focal plane. A positive angle value increases counterclockwise from the horizontal x-axis. In the initial plane, the light field has only linear polarization directed along the vertical y-axis, and the Jones vector (1) does not depend on the polar angle φ. In Eqs. (1.2) and (1.3), angle θ is the tilt angle of the rays to the optical axis, θ_0 is the maximal tilt angle, determining the numerical aperture NA, z is the direction of the optical axis, $z = 0$ is the focal plane, k is the wavenumber of light, (x, y) are the Cartesian coordinates in the cross sections of the light beam converging into the focus (x is the horizontal axis, y is the vertical axis). The initial amplitude function $A(\theta)$ (suppose it is a real function) can be constant (plane wave) or in the form of a Gaussian beam. From (1.2), one can obtained the intensity distributions of each component of the electric vector

$$\begin{aligned}
I_x &= I_{2,2}^2\sin^2(2\varphi),\\
I_y &= I_{0,0}^2 + I_{2,2}^2\cos^2(2\varphi) - 2I_{0,0}I_{2,2}\cos(2\varphi),\\
I_z &= 4I_{1,1}^2\sin^2(\varphi).
\end{aligned} \tag{1.4}$$

We note that formulae (1.1)–(1.4) differ from the formulae obtained in [1], since the initial field (1.1) is polarized along the y-axis, whereas in [1] the initial field was polarized along the x-axis. Despite the initial light field (1.1) has only one component E_y, Maxwell's equations indicate that, upon light propagation, all three components of the E-field appear. If the light field propagates at a small angle to the optical axis, then the other two field components (E_x and E_z) are small and can be neglected. At tight focusing, light propagates at large angles to the optical axis, so that all three components of the E-field (1.2) have a comparable value [15, 16]. It can be seen from (1.1) that the intensity distribution I_x of the horizontal projection of the electric vector in the plane of focus will have the form of four local maxima (light spots), the centers of which are located on a circle centered on the optical axis and lying on the rays emanating from the center at angles $\varphi = \pi/4, 3\pi/4, 5\pi/4, 7\pi/4$.

The intensity distribution I_y will have the form of an almost circular spot with a maximum on the optical axis $I_y = I_{0,0}^2$. The difference from the round shape of the spot arises from the fact that the distribution of intensity I_y along the vertical axis ($\varphi = \pi/2$) will be greater ($I_y = \left(I_{0,0} + I_{2,2}\right)^2$) than along the horizontal axis ($\varphi = 0$, $I_y = \left(I_{0,0} - I_{2,2}\right)^2$). Intensity distribution (1.4) at the focus of the longitudinal component of the electric vector I_z will have the form of two light spots, the centers of which lie on the vertical axis. This type of intensity distribution of electric vector individual components leads to the fact that the distribution of the total intensity at the focus has the form of an ellipse elongated along the vertical axis:

$$I = I_x + I_y + I_z = I_{0,0}^2 + I_{2,2}^2 + 2I_{1,1}^2 - 2\left(I_{1,1}^2 + I_{0,0}I_{2,2}\right)\cos(2\varphi). \tag{1.5}$$

Let us find the longitudinal component of the spin angular momentum (SAM) vector near the field focus (1.1) using the formula [17]:

$$\boldsymbol{S} = \left(\frac{c^2\varepsilon_0}{2\omega}\right)\mathrm{Im}\left(\boldsymbol{E}^* \times \boldsymbol{E}\right) \tag{1.6}$$

where c is the speed of light in vacuum, ω is the angular frequency of the monochromatic light, ε_0 is the vacuum permittivity, Im is the imaginary part of the number, $\times$ is the sign of vector multiplication, * is the sign of complex conjugation. Below, we omit the constant $[(c^2\varepsilon_0)/(2\omega)]$ for brevity. We note that sometimes, due to the electric–magnetic democracy, Eq. (1.6) is written with two terms rather than one: $[c^2/(2\omega)]\mathrm{Im}\left[\varepsilon_0(\boldsymbol{E}^* \times \boldsymbol{E}) + \mu_0(\boldsymbol{H}^* \times \boldsymbol{H})\right]$, with μ_0 being the vacuum permeability ($c^2\varepsilon_0 = \mu_0^{-1}$). However, immediately from the expression for the Poynting vector, only one term is obtained either for the E-vector or for the H-vector [17]. In addition, due to different constants, both terms will give different contribution to the components of the SAM vector. Thus, expression (1.6) is correct. Substituting from (1.2) into (1.6), we will assume that integrals (1.3) are complex, since z is different from zero. We get:

$$S_z = 2\mathrm{Im}\left(E_x^* E_y\right) = 2\sin(2\varphi)\mathrm{Im}\left(I_{2,2}^*\left(I_{0,0} - \cos(2\varphi)I_{2,2}\right)\right) \tag{1.7}$$

Certainly, near the tight focus, all 6 components of the E- and H-vectors (1.2) are significant, and none of these components can be neglected. Therefore, similarly to Eq. (1.7), we can write expressions for the components S_x and S_y:

$$S_x = 2\mathrm{Im}\left(E_y^* E_z\right) = 4\sin(\varphi)\mathrm{Re}\left(I_{1,1}\left(\cos(2\varphi)I_{2,2}^* - I_{0,0}^*\right)\right),$$
$$S_y = 2\mathrm{Im}\left(E_z^* E_x\right) = 4\sin(\varphi)\sin(2\varphi)\mathrm{Re}\left(I_{1,1}^* I_{2,2}\right). \quad (1.8)$$

Let us single out the real and imaginary parts of the integrals included in (1.7) $I_{0,0} = R_0 + iI_0$, $I_{2,2} = R_2 + iI_2$. Then, instead of (1.7), we write:

$$S_z = 2\sin(2\varphi)(I_0 R_2 - I_2 R_0) \quad (1.9)$$

The integrals R_0, R_2 in (1.9) include the co-multiplier $\cos(kz\cos\theta) \approx 1$ at $kz \ll 1$, and the integrals I_0 , I_2 include the co-multiplier $\sin(kz\cos\theta) \approx kz\cos\theta$ at $kz \ll 1$. With this in mind, instead of (1.9), we write:

$$S_z \approx 2kz\sin(2\varphi)\left(\overline{I}_0\overline{R}_2 - \overline{I}_2\overline{R}_0\right). \quad (1.10)$$

In (1.10), the following notations are used:

$$\overline{R}_0 = I_{0,0}(z=0), \overline{R}_2 = I_{2,2}(z=0),$$
$$\overline{I}_0 = \overline{I}_{0,0}(z=0), \overline{I}_2 = \overline{I}_{2,2}(z=0),$$
$$\overline{I}_{\nu,\mu} = \left(\frac{4\pi f}{\lambda}\right)\int_0^{\theta_0} \sin^{\nu+1}\left(\frac{\theta}{2}\right)\cos^{3-\nu}\left(\frac{\theta}{2}\right)\cos^{3/2}(\theta)A(\theta)\mathrm{e}^{ikz\cos\theta}J_\mu(x)\mathrm{d}\theta. \quad (1.11)$$

Let on a circle of some radius the expression in parentheses in (1.10) be greater than zero $\overline{I}_0\overline{R}_2 - \overline{I}_2\overline{R}_0 > 0$, and since $\sin(2\varphi)$ in (1.10) is positive in 1 and 3 quadrants, and negative in 2 and 4, then before the focus ($z < 0$) the longitudinal component SAM S_z in (1.10) will be positive in 2 and 4 quadrants, and negative in 1 and 3. And since the sign of the entire expression after focus ($z > 0$) will change to the opposite, the longitudinal component of SAM S_z in (1.9) will be positive in 1 and 3 quadrants, and negative in 2 and 4. This means that before the focus in the 2 and 4 quadrants the polarization vector will rotate counterclockwise (right circular or elliptical polarization), and after focus in these quadrants, the polarization vector will rotate clockwise (left circular or elliptical polarization). Recall that in the plane of focus, the light at each point has only linear polarization, since at $z = 0$ the longitudinal component of the SAM S_z in (1.10) is equal to zero. The defocusing magnitude z in Eq. (1.10) affects the size of the areas in the transverse plane, where polarization is not linear. At a distance z nearly equal to λ, the size of the circular polarization area is maximal (for NA = 0.95 it is approximately $\lambda/2$). As z tends to zero (i.e., in the focus), the size of the area with circular polarization decreases to zero.

Note also that the longitudinal component of the SAM is exactly equal to the third component of the Stokes vector:

$$S_z = 2\mathrm{Im}\left(E_x^* E_y\right) = s_3, \tag{1.12}$$

which shows the presence of circular and elliptical polarization in the light field. In the next section, the presented theoretical predictions will be confirmed by simulation. We note that the change in the rotation direction of the polarization vector to the opposite beyond the focal plane, as follows from Eq. (1.10), can be explained by the angular momentum (AM) conservation law. Since polarization in the initial plane and in the focal plane is locally linear, $S_z = 0$. Therefore, if there are areas with left-handed circular polarization before the focus, then beyond the focus, circular polarization in these areas should become right-handed. However, the presence of such areas near the focus does not follow from the AM conservation.

1.1.2 Simulation by Richards-Wolf Formula

In this work, using the Richards-Wolf formulas, focusing of a linearly polarized plane wave (wavelength 633 nm) was simulated by choosing a lens with NA = 0.95. The field near the tight focus was calculated using the integrals [1]:

$$\begin{aligned} \boldsymbol{U}(\rho, \psi, z) = -\frac{if}{\lambda} \int_0^{\theta_0} \int_0^{2\pi} & B(\theta, \varphi) T(\theta) \boldsymbol{P}(\theta, \varphi) \\ & \times \exp\{ik[\rho \sin\theta \cos(\varphi - \psi) + z\cos\theta]\} \\ & \sin\theta d\theta d\varphi, \end{aligned} \tag{1.13}$$

where $\mathbf{U}(\rho, \psi, z)$ is the strength of the electric or magnetic field, $B(\theta, \varphi)$ is the electric or magnetic field at the input of the wide-aperture system in coordinates of the exit pupil (θ is the polar angle, φ is the azimuthal angle), $T(\theta)$ is the lens apodization function, f is the focal length, $k = 2\pi/\lambda$ is the wavenumber, λ is the wavelength (in the simulation it was considered equal to 633 nm), θ_0 is the maximum polar angle determined by the numerical aperture of the lens ($\mathrm{NA} = \sin\theta_0$), $\mathbf{P}(\theta, \varphi)$ is the polarization vector, for the strength of the electric and magnetic fields has the form:

$$\begin{aligned} \boldsymbol{P}(\theta, \varphi) = & \begin{bmatrix} 1 + \cos^2\varphi(\cos\theta - 1) \\ \sin\varphi\cos\varphi(\cos\theta - 1) \\ -\sin\theta\cos\varphi \end{bmatrix} a(\theta, \varphi) \\ & + \begin{bmatrix} \sin\varphi\cos\varphi(\cos\theta - 1) \\ 1 + \sin^2\varphi(\cos\theta - 1) \\ -\sin\theta\sin\varphi \end{bmatrix} b(\theta, \varphi), \end{aligned} \tag{1.14}$$

where a (θ, φ) and b (θ, φ) are functions describing the polarization state of the x- and y-components intensities of the focused beam. In contrast to formulae (1.2) and (1.3), we gave Eqs. (1.13) and (1.14) in a general form to show that further modeling is carried out by the general formulae (1.13), (1.14) and that the simulation results confirm the theoretical conclusions, following from the expressions (1.11), (1.12). After calculating the components of the electric field, the behavior of the components of the Stokes vector near the sharp focus was calculated. The Stokes vector components are calculated using the formulas:

$$\begin{aligned} s_0 &= E_x E_x^* + E_y E_y^*, \\ s_1 &= E_x E_x^* - E_y E_y^*, \\ s_2 &= 2\mathrm{Re}\big(E_x^* E_y\big), \\ s_3 &= 2\mathrm{Im}\big(E_x^* E_y\big). \end{aligned} \tag{1.15}$$

Similarly to the expressions (1.7)–(1.9), substitution of Eq. (1.2) into Eq. (1.15) allows obtaining explicit expressions for the Stokes components s_1 and s_2 near the focus. For instance, more simple expression is derived for s_2 at $kz \ll 1$:

$$s_2 \approx 2\sin(2\varphi)\overline{R}_2\big(\overline{R}_0 - \overline{R}_2\cos(2\varphi)\big). \tag{1.16}$$

At small $kz \ll 1$, the second Stokes component (1.16) does not depend on z and therefore does not change sign when passing through the focus ($z = 0$). Below, this is confirmed by simulation. Similarly, the first Stokes component s_1 in Eq. (1.15), expressed via the components of the E-vector (1.2), is also independent of z near the focus.

To estimate the relative contribution of individual polarization components, it is convenient to use the Stokes vector components normalized to the transverse intensity: $(S_1, S_2, S_3) = \big(s_1/s_0, s_2/s_0, s_3/s_0\big)$. It is known that when focusing light of linear polarization at the focus, all three components of the electric field strength are observed [18]. Figure 1.1 illustrates the distribution of the total intensity and its individual components in the focus of an aplanatic lens with NA = 0.95 when focusing a plane wave with a wavelength of 633 nm and polarization along the y-axis. To estimate the effect of defocusing, Fig. 1.2 shows the same distributions of the total intensity and of the individual intensity components as in Fig. 1.1, but at a distance λ from the focal plane. The intensity distributions have the same shape at the same distance before and after the focus.

Figure 1.1 shows that the initial component makes the main contribution to the focal spot formation, but the longitudinal component of the intensity also begins to make a significant contribution. The component perpendicular to the input polarization is rather small but present, while the light at the focus is still linearly polarized. Note that the distributions of the total intensity at the focus and the intensity of individual components in Fig. 1.1 confirm the theoretical predictions that follow from

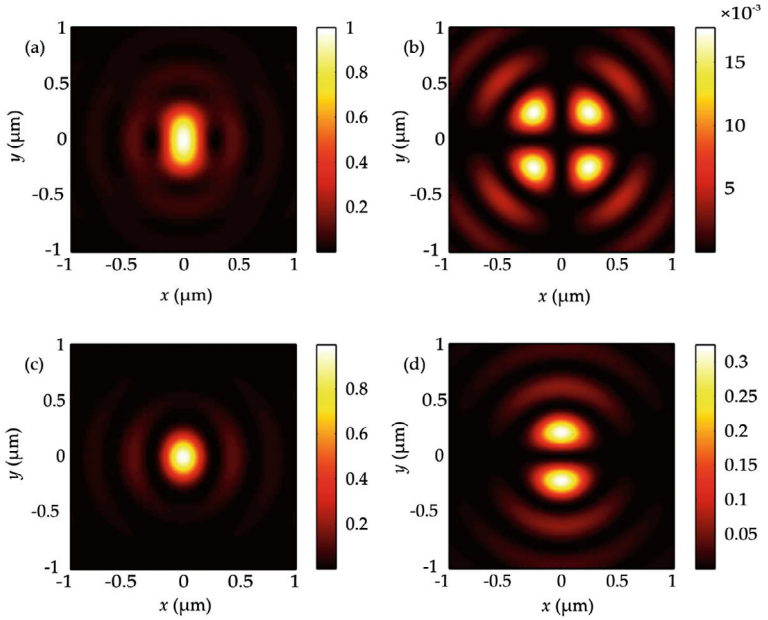

Fig. 1.1 Distribution of the total intensity $I_x + I_y + I_z$ (**a**) and individual components of the intensity I_x (**b**), I_y (**c**), I_z (**d**) in the plane of focus

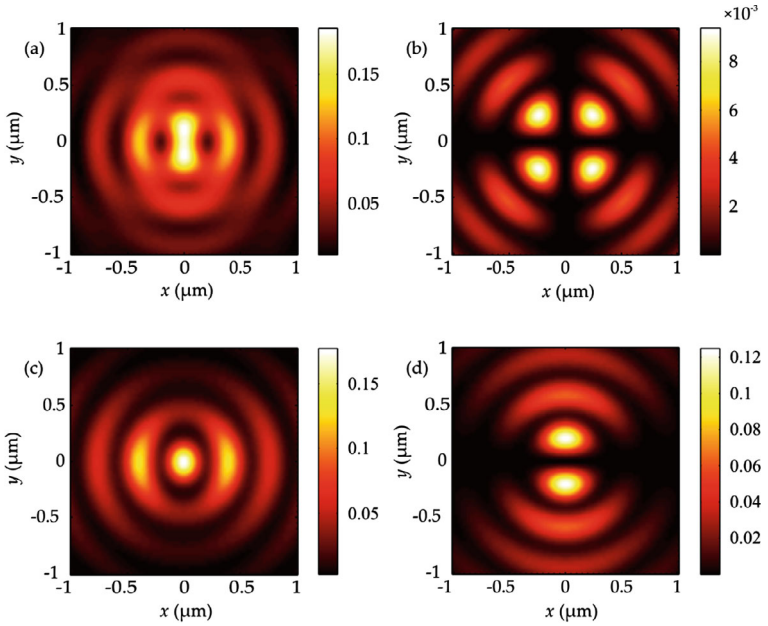

Fig. 1.2 Distribution of the total intensity $I_x + I_y + I_z$ (**a**) and individual components of the intensity I_x (**b**), I_y (**c**), I_z (**d**) at a distance λ after the focus

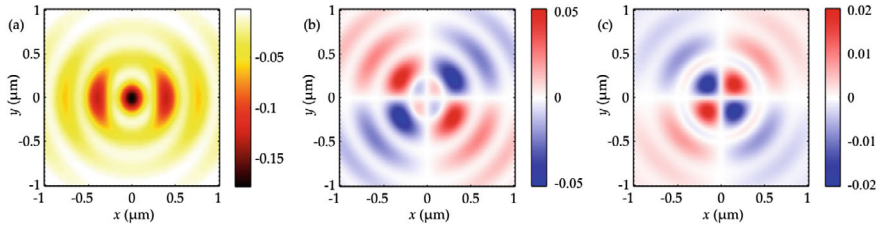

Fig. 1.3 Distribution of the Stokes vector components s_1 (**a**), s_2 (**b**) and s_3 (**c**) at a distance λ after the focus

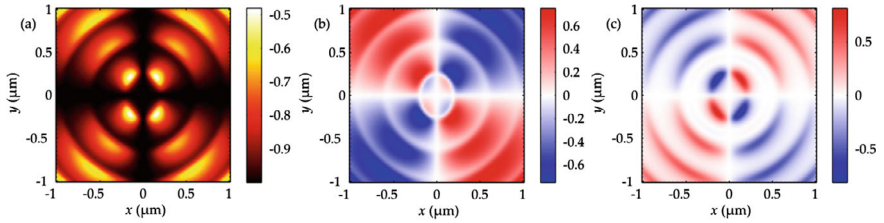

Fig. 1.4 Distribution of the components of the normalized Stokes vector S_1 (**a**), S_2 (**b**) and S_3 (**c**) at a distance λ after the focus

expressions (1.4) and (1.5). Figure 1.2 indicates that a small shift from the focal plane (by a distance λ) leads to decrease of the maximum intensity 5 times.

The distribution of the components of the Stokes vector (s_1, s_2, s_3) and the normalized components of the Stokes vector (S_1, S_2, S_3) at the distance $z = \lambda$ after the focus is shown in Figs. 1.3 and 1.4, respectively.

From Figs. 1.3 and 1.4, it can be seen that the polarization after focus is predominantly linear. In the center of the focal spot in Fig. 1.3a, a minimum is observed, which indicates that the polarization at the focus is directed along the y-axis. This is also confirmed by Fig. 1.4a: for a wave fully polarized along the y-axis $S_1 = -1$. From Fig. 1.4a can be seen that the polarization does not change its direction at the focus and along the x and y axes, but along the straight lines located at an angle of ± 45° to the axes, the deviation from the initial polarization turns out to be maximum. From Figs. 1.3 and 1.4, it is also seen that the diverging beam contains regions with circular polarization. Recall that there are no such regions at the focus itself—the light is linearly polarized. From Fig. 1.4c it is seen that the contribution of circular polarization in such regions is quite noticeable—for $S_3 = \pm 1$ the polarization is completely circular, but here in some regions S_3 reaches values of ± 0.8.

Figures 1.5and 1.6 similarly show the distribution of the Stokes vector and normalized Stokes vector at a distance of one wavelength in front of the focus.

Comparison of Figs. 1.4 and 1.6 shows that the first two components of the Stokes vector describing linear polarization have not changed, and the third has changed its sign to the opposite. After passing the plane of the focus, the direction of circular (elliptical) polarization is reversed—for example, in the first quarter, the light in front

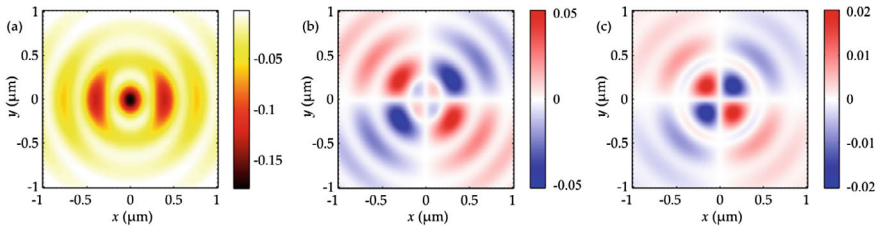

Fig. 1.5 Stokes vector components s_1 (**a**), s_2 (**b**), and s_3 (**c**) at a distance λ before the focal plane

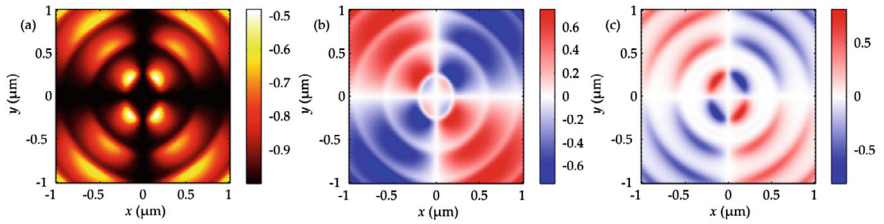

Fig. 1.6 Distribution of the components of the normalized Stokes vector S_1 (**a**), S_2 (**b**) and S_3 (**c**) at a distance λ before the focal plane

of the focus plane was with left circular polarization, and after focus—with right polarization. Before the focus, the right circular (elliptical) polarization appears in the 2nd and 4th quadrants and the left circular polarization appears in the 1st and 3rd quadrants (Fig. 1.6c). It agrees with the theoretical prediction based on expression (1.10). And the change in the direction of rotation of the polarization vector in these quadrants after passing through the focus also follows from (1.10).

Below we show how the distribution of S_3 changes with the distance from the focal plane. Figure 1.7 shows the intensity distribution (Fig. 1.7a) and the longitudinal Stokes component S_3 (Fig. 1.7b) in the longitudinal plane yz along the z-axis, rotated by an angle $\varphi = 45°$ (i.e., passing through the S_3 maximum in Fig. 1.6).

Figure 1.7 demonstrates that in the focal plane, the light field is linearly polarized. However, directly beyond the focal plane, areas with elliptical polarization are generated (red areas in Fig. 1.7). It is also interesting that as we move away from the

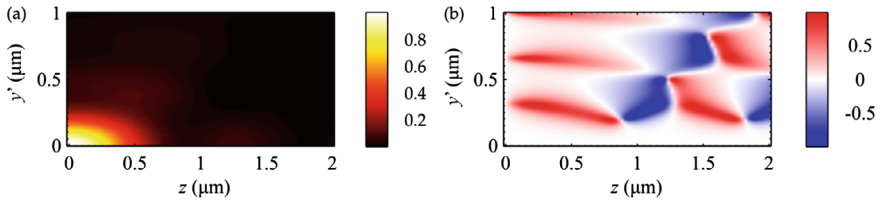

Fig. 1.7 Distributions of the intensity and of the third Stokes component in the longitudinal plane yz along the z-axis (by an angle 45°)

focus, direction of rotation of the polarization vectors changes to the opposite (blue areas in Fig. 1.7). Figure 1.7b also shows how the size of the area with elliptical polarization changes with the distance z.

1.1.3 Modeling the Formation of Circular Polarization Using the FDTD Method

To check the correctness of calculations by the Richards-Wolf formulas, an additional simulation was performed using the FDTD method. Focusing of a linearly polarized plane wave ($\lambda = 633$ nm) by a Fresnel zone plate with a focal length of $f = 500$ nm and a diameter of 7.9 μm was considered. The numerical aperture of such a lens is NA = 0.99. Focusing was simulated using the FDTD method implemented in the FullWave software. Note that the FDTD method implemented in FullWave makes it possible to calculate the values of the electromagnetic field components at individual moments of time. To calculate the complex amplitude on the basis of individual instantaneous values of the field amplitudes, the method proposed in [19] was used. Figure 1.8 shows the distribution of the components of the normalized Stokes vector at a distance of one wavelength after the focus.

From Fig. 1.8, it can be seen that simulating using the FDTD method confirms the results obtained using the Richards-Wolf formulas. In particular, Fig. 1.8a shows that light is predominantly linearly polarized along the y-axis, and Fig. 1.8c shows that quadrants 1 and 3 contain right-handed circular polarization, and quadrants 2 and 4—left.

Comparison of Figs. 1.4 and 1.8 indicates that although the structures of both patterns are similar, there are also significant differences. This is because the simulations by the Richards-Wolf method [1] and by the FDTD method [19] were carried out under different conditions. In the latter case, tight focusing of light was simulated by passing the light field through a real Fresnel zone plate with a focal length equal to the wavelength ($f = \lambda$) and with a numerical aperture NA = 0.99. At the same time, the Richards-Wolf formalism adequately describes the light field at the focus of an ideal spherical lens if $f \gg \lambda$. Thus, the Richards-Wolf formalism approximately

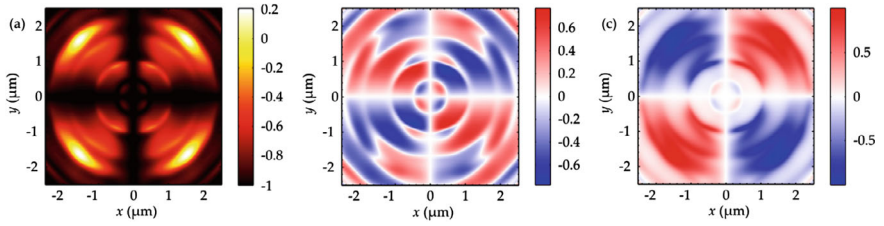

Fig. 1.8 Components of the Stokes vector S_1 (**a**), S_2 (**b**) and S_3 (**c**) when calculating using the FullWAVE software at a distance of $z = 0.65$ μm after the actual focus

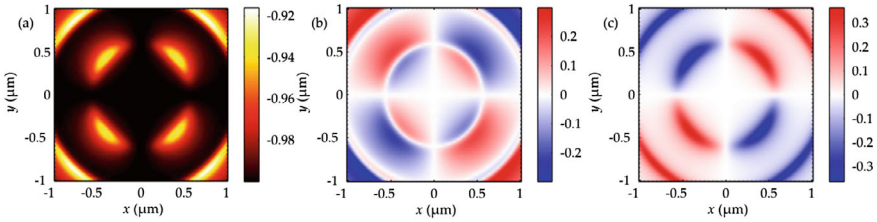

Fig. 1.9 Distribution of the components of the normalized Stokes vector S_1 (**a**), S_2 (**b**) and S_3 (**c**) for a lens with a numerical aperture NA = 0.6

describes the behavior of light near the focus, whereas the FDTD method, based on a rigorous solution of the Maxwell equations, adequately describes the behavior of light at the focus near the surface of the focusing zone plate. Therefore, modeling by the FDTD method expands the boundaries of the discovered optical phenomenon: generation of local areas with circular (elliptical) polarization near the tight focus of light with initially linear polarization.

1.1.4 Reducing the Contribution of Circular Polarization with Decreasing Numerical Aperture of the Lens

Let us now consider the contribution of reducing the numerical aperture of the lens to NA = 0.6 (corresponding to a standard 40 × aplanatic lens). The result is shown in Fig. 1.9. Figure 1.9 shows that the maximum S_3 has decreased by 2 times. And from Fig. 1.9a, it can be seen that the relative contribution of linear polarization (along the *y*-axis) increased significantly: the maximum in Fig. 1.4 was equal to − 0.5, and in Fig. 1.9a to − 0.92. Recall that for $S_1 = \pm 1$, the polarization is completely linear.

1.1.5 Calculation of the Moment of Forces Acting on a Dielectric Microparticle Near the Focus

Let us calculate a force and a torque, acting onto a microbed from the light field. The force **F** and the torque **M** relative to an arbitrary point A, are equal to [20, 21].

$$\boldsymbol{F} = -\oint_S (\sigma \cdot \boldsymbol{n}) \mathrm{d}S \tag{1.17}$$

$$\boldsymbol{M} = \oint_S [\boldsymbol{r} \times (\sigma \cdot \boldsymbol{n})] \mathrm{d}S \tag{1.18}$$

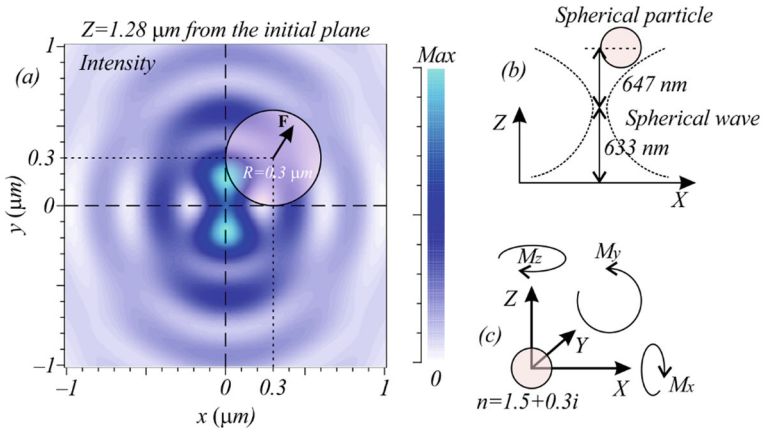

Fig. 1.10 Intensity pattern (**a**) and a spherical bed with radius $R = 0.3$ μm. The position of the bed is $x_p = 0.3$ μm, $y_p = 0.3$ μm. Shown at the right are a schematic position of the bed (**b**) and directions of the positive torques values along *x, y* and *z* axis (**c**)

where **r** is the radius-vector from the point $A(x, y, z)$ to the point of integration on the surface S, **n** is an external normal vector to the surface S, A is the point relative to which the torque **M** is calculated, and σ is the Maxwell stress tensor, the components of which in the CGS system can be written [22]

$$\sigma_{ik} = \frac{1}{4\pi}\left(\frac{|\boldsymbol{E}|^2 + |\boldsymbol{H}|^2}{2}\delta_{ik} - E_i E_k - H_i H_k\right) \tag{1.19}$$

where E_i, H_i are the electric and magnetic field components and δ_{ik} is the Kronecker symbol ($\delta_{i=k} = 1$, $\delta_{i\neq k} = 0$).

Shown in Fig. 1.10 is a simulation result of the torque and force calculation acting on the spherical microbed.

Calculations show that for the position of the particle $x_p = 0.3$ μm, $y_p = 0.3$ μm the force projections are $F_x = 2.79$ pN, $F_y = 3.7$ pN, $F_z = 8.78$ pN. The torque projections are $M_x = 2.81 \cdot 10^{-19}$ Nm, $M_y = -5.55 \times 10^{-19}$, $M_z = 1.73 \times 10^{-19}$ Nm. If shift the bed at the position $x_p = 0.3$ μm, $y_p = -0.3$ μm, then the result force projections will be $F_x = 2.66$ pN, $F_y = -3.58$ pN, $F_z = 8.9$ pN, and the torque projections will be $M_x = -3.0 \times 10^{-19}$ Nm, $M_y = -5.9 \times 10^{-19}$, $M_z = -1.5 \times 10^{-19}$ Nm. Figure 1.10 shows that in the first quadrant the axial moment of forces is positive ($M_z = 1.73 \times 10^{-19}$), and in the fourth quadrant the moment of forces is negative ($M_z = -1.5 \times 10^{-19}$). This proves that the longitudinal projection of the SAM is positive in the first quadrant and negative in the fourth (Figs. 1.8 and 1.9).

In this section, theoretically, using the Richards-Wolf formalism and using two different modeling methods, it was shown that with sharp focusing of light with linear polarization in the planes before and after the focus, there are regions that arise in pairs in even and odd quadrants, and in which light is circularly or elliptically polarized

(e.g., even to the right and to the odd to the left) [22]. Moreover, after passing through the focus in these areas, the direction of rotation of the polarization vector changes to the opposite (in even quadrants, it is now left-handed, and in odd quadrants, it is right-handed circular or elliptical polarization). This result allows the use of linearly polarized light to rotate microparticles (the size of the circularly polarized region is about 0.6 μm by 0.6 μm) around its center of mass. We note that a similar result has been obtained in [23]. It has been shown that certain structures allow generating before the focus and beyond the focus two conjugate optical vortices with opposite-sign topological charges and with longitudinal axial polarization. In our work, we have not used any additional structures.

1.2 Focusing a Vortex Laser Beam with Polarization Conversion

When strongly focusing a circularly polarized Gaussian beam, a near-focus orbital energy flow has been generated thanks to spin-orbital conversion [24–30]. In the original plane, such a beam has no orbital angular momentum (OAM), only having a non-zero on-axis projection of the spin angular momentum (SAM) vector thanks to circular polarization. However, a non-zero longitudinal component of the electric vector that occurs in the strong focus leads to the generation of a transverse energy flow, which produces the non-zero longitudinal OAM component. Behavioral patterns of SAM and OAM in the tight focus of optical vortices were studied in [31–35]. On the other hand, there have been publications concerned with a reverse energy flow in the tight focus of optical vortices [1, 10, 36, 37] and some laser beams, like vector X-waves [38], non-paraxial Airy beams [39], Weber beams [40], vector Bessel beams [41], and fractional Bessel vortex beams [42].

In this section, using Richards-Wolf formulae, we derive analytical relationships to describe projections of the Poynting vector (the energy flow) and the SAM vector when tightly focusing a linearly polarized optical vortex with the topological charge 2. In the original plane, all SAM vector components of such a beam are zero, but they all become non-zero near the strong focus. This can be explained by the effect inverse to the spin-orbital conversion. Thus, in the case under study, thanks to the orbital-spin conversion, the original linearly polarized vortex beam generates a circularly polarized vortex beam in the tight focus. It is important to mention that a vortex beam with the topological charge (TC) $m = 2$ has a specific feature—that of generating an on-axis reverse energy flow in the tight focus (characterized by the negative longitudinal projection of the Poynting vector). Besides, there will be non-zero on-axis intensity. At any $m > 2$, except for $m = 1$ and $m = 2$, both the on-axis intensity of light and energy flow are zero.

We note that for spin-orbital coupling to occur the beam needs to propagate in a medium and because of this throughout the text below, we use the notion of spin-orbital conversion. Thanks to the beam rays converging to the focus, there

appears a non-zero longitudinal projection of the electric field vector that, combined with the transverse components, produces a transverse energy flow (although the original energy flow has only a longitudinal component), which, in turn, produces a longitudinal projection of the OAM vector. In the focus, two transverse projections of the electric field vector have a relative phase shift of $\pi/2$, generating a circularly polarized beam, which, in turn, generates the longitudinal component of the SAM vector.

1.2.1 Energy Flow and SAM in the Strong Focus

Previously, relationships to describe projections of the electric and magnetic fields in the vicinity of the tight focus of an original linearly polarized optical vortex with an arbitrary integer TC m have been derived [29]. In this case, a near-axis reverse energy flow in the focus was shown to occur at any $m \geq 2$. However, with the reverse energy flow being maximal on the optical axis only at $m = 2$, below, we look into focusing a linearly polarized optical vortex with TC $m = 2$. Based on the Richards-Wolf theory [1], it is possible to derive projections of the electric field vector in the tight focus of an aplanatic optical system. If the original light field is given by

$$\boldsymbol{E} = A(\theta)\mathrm{e}^{i2\varphi}\begin{pmatrix}1\\0\end{pmatrix}, \boldsymbol{H} = A(\theta)\mathrm{e}^{i2\varphi}\begin{pmatrix}0\\1\end{pmatrix} \tag{1.20}$$

where **E** and **H** are the electric and magnetic field of Jones vectors, projections of the electric field vector in the focal plane will be given by [29]

$$\begin{aligned}
E_x &= i\mathrm{e}^{2i\varphi}\left(I_{0,2} + \frac{1}{\sqrt{2}}\mathrm{e}^{2i\varphi}I_{2,4} + \frac{1}{\sqrt{2}}\mathrm{e}^{-2i\varphi}I_{2,0}\right),\\
E_y &= -\mathrm{e}^{2i\varphi}\left(-\frac{1}{\sqrt{2}}\mathrm{e}^{2i\varphi}I_{2,4} + \frac{1}{\sqrt{2}}\mathrm{e}^{-2i\varphi}I_{2,0}\right),\\
E_z &= 2\mathrm{e}^{2i\varphi}\left(\frac{1}{\sqrt{2}}\mathrm{e}^{i\varphi}I_{1,3} - \frac{1}{\sqrt{2}}\mathrm{e}^{-i\varphi}I_{1,1}\right),
\end{aligned} \tag{1.21}$$

where

$$I_{\nu,\mu} = \left(\frac{4\pi f}{\lambda}\right)\int_0^{\theta_0}\sin^{\nu+1}\left(\frac{\theta}{2}\right)\cos^{3-\nu}\left(\frac{\theta}{2}\right)\cos^{1/2}(\theta)A(\theta)\mathrm{e}^{ikz\cos\theta}J_\mu(x)\mathrm{d}\theta, \tag{1.22}$$

and λ is the incident wavelength, f is the focal length of the aplanatic system, $x = kr\sin\theta$, $J_\mu(x)$ is the first-kind Bessel function, and $NA = \sin\theta_0$ is the numerical aperture. Assuming the initial amplitude $A(\theta)$ to be a real function, it can be given by a constant (plane wave) or a Gaussian beam

$$A(\theta) = \exp\left(\frac{-\gamma^2 \sin^2\theta}{\sin^2\theta_0}\right) \tag{1.23}$$

where γ is constant. We seek to derive projections of the SAM vector

$$\boldsymbol{S} = \frac{1}{2}\mathrm{Im}\left[\boldsymbol{E}^* \times \boldsymbol{E}\right] \tag{1.24}$$

where Im is the imaginary part of the number, $\mathbf{E}^*$ denotes complex conjugation of the electric field vector, ×—vector multiplication sign. Substituting (1.21) into (1.24) yields expressions for projections of the SAM vector in the focal plane ($z = 0$) for an initially linearly polarized optical vortex ($m = 2$), Eq. (1.20):

$$\begin{aligned}
S_x &= \left(I_{1,1}I_{2,0} - I_{1,3}I_{2,4}\right)\sin\varphi + \left(I_{1,1}I_{2,4} - I_{1,3}I_{2,0}\right)\sin 3\varphi,\\
S_y &= -\left(I_{1,1}I_{2,0} - I_{1,3}I_{2,4}\right)\cos\varphi -\\
&\quad - \left(I_{1,1}I_{2,4} - I_{1,3}I_{2,0}\right)\cos 3\varphi - \sqrt{2}I_{2,0}\left(I_{1,1} - I_{1,3}\right)\cos\varphi,\\
S_z &= \frac{1}{2}\left(I_{2,0} - I_{2,4}\right)\left(I_{2,0} + I_{2,4} + \sqrt{2}I_{0,2}\cos 2\varphi\right).
\end{aligned} \tag{1.25}$$

From Eq. (1.25), the on-axis longitudinal projection of the SAM vector is seen to be non-zero and positive:

$$S_z(r = z = 0) = \frac{1}{2}I_{2,0}^2. \tag{1.26}$$

This means that the light wave in the focus near the optical axis has right-handed circular polarization (electric vector rotates anticlockwise). From the last equation in (1.25) the light is also seen to be inhomogeneously polarized in the focal plane. For instance, light will be linearly polarized on the radii where the inequality $I_{2,0} = I_{2,4}$ holds, because $S_z = 0$. Meanwhile, in the regions where $S_z < 0$, the light wave will be left-handed circularly polarized. Along the rays in the focal plane outgoing from the center at angles φ: $\pi/4$, $3\pi/4$, $5\pi/4$, and $7\pi/4$, alternating polarization states will occur: being right-handed circular at $I_{2,0}^2 > I_{2,4}^2$, linear at $I_{2,0}^2 = I_{2,4}^2$, and left-handed circular at $I_{2,0}^2 < I_{2,4}^2$. From the first two equations of Eq. (1.25), it is seen that at $\varphi = \pi n$, $n = 1, 2, \ldots$ $S_x = 0$ and at $\varphi = \pi/2 + \pi n$, $n = 1, 2, \ldots$ $S_y = 0$. This means that in the longitudinal planes yz and xz, light is circularly (or elliptically) polarized near the strong focus.

Next, let us consider expressions for projections of the Poynting vector (energy flow) $\boldsymbol{P} = \frac{1}{2}\mathrm{Re}\left[\boldsymbol{E}^* \times \boldsymbol{H}\right]$ in the focal plane when focusing an optical vortex ($m = 2$) with linear original polarization (1.20):

$$\begin{aligned}
P_x &= -Q(r)\sin\varphi,\\
P_x &= Q(r)\cos\varphi,
\end{aligned}$$